

Article

Enhanced Phosphorus Release from Phosphate Rock Activated with Lignite by Mechanical Microcrystallization: Effects of Several Typical Grinding Parameters

Xian-mei Zhang ^{1,2,*} , Yi Li ³, Cheng Hu ¹, Zhen-quan He ^{2,4}, Ming-xing Wen ¹, Guo-sheng Gai ^{2,*}, Zhao-hui Huang ¹, Yu-fen Yang ^{2,4}, Xiang-Yang Hao ¹ and Xiao-yan Li ⁵

¹ School of Materials Science and Technology, Beijing Key Laboratory of Materials Utilization of Nonmetallic Minerals and Solid Wastes, National Laboratory of Mineral Materials,

China University of Geosciences (Beijing), Beijing 100083, China; huchengzll123@163.com (C.H.); wenmingxing12138@163.com (M.-x.W.); huang118@cugb.edu.cn (Z.-h.H.); haoxy@cugb.edu.cn (X.-Y.H.)

² School of Materials Science and Engineering, Tsinghua University, Beijing 100084, China;

hezhenquan@chinapowder.com (Z.-q.H.); 13691133052@139.com (Y.-f.Y.)

³ School of Materials and metallurgy, Guizhou University, Guiyang 550025, China;

cugb1003142129liyi@163.com

⁴ Zibo Tsingda Powder Material Engineering Co, Ltd., Zibo 255000, China

⁵ Tianjin cement industry design and research institute Co. Ltd., Tianjin 300400, China;

lixiaoyan@sinoma-tianjin.cn

* Correspondence: zhangxianmei@chinapowder.com (X.-m.Z.); gaigs@tsinghua.edu.cn (G.-s.G.)

Received: 12 January 2019; Accepted: 13 February 2019; Published: 18 February 2019



Abstract: Recently, microcrystallization technology has gained much interest because of the enhanced dissolution of the target sample and promotion of the sustainable development of agriculture. Phosphorus (P) is one of the most important nutrients for increasing crop yield; the increase in effective P ratio directly from raw phosphate rock (PR) powder by mechanical grinding to increase its microcrystallinity is believed to be the best choice for this purpose. This study reports the improvement in the activation property of PR powder with different lignite ratios (1%, 2%, 3%, and 5%), particularly the relationship between particle-size distribution, specific surface area, granule morphology, and the citric acid-soluble P. It was found that a 3% lignite addition was the optimal treatment for increasing the release of citric acid-soluble P. The maximum total amount of dry matter from rapeseed cultivation and the available P after the test increased by 56.1% and 89.6%, respectively, with direct use of PR and microcrystallized PR powder (PR2), compared with the control test without any addition of phosphate minerals.

Keywords: microcrystallinity; medium-low-grade phosphate mineral; lignite; citric acid soluble

1. Introduction

Phosphorus (P) deficiency is a common phenomenon in agricultural soils worldwide. Despite long-term application of phosphate fertilizers to increase crop yields, P availability is often low due to the high affinity of phosphate to the soil solid phase. Worldwide, ~80% of phosphate rock (PR) is mined for phosphate fertilizer production [1]. PR resources play a significant role in supporting the sustainable development of agriculture [2,3]. Most natural phosphate minerals are medium-low-grade; it is not easy to concentrate them for the production of phosphate fertilizer. Weathering rubber phosphate ($\omega \text{ P}_2\text{O}_5 \leq 20\%$) is a typical refractory medium-low-grade mineral [4]. PR is an important natural source of P for plant nutrition, but the low solubility and availability of P

from PR limits its application in agriculture [5,6]. With the rapid depletion of high-grade PR resources, improvement of the utilization rate of medium-low-grade PR powder is the only way to increase organic food production and achieve sustainable development of the efficient slow-release phosphate fertilizer industry [7].

In recent years, mechanochemistry has been widely applied in the direct processing of medium-low-grade PR. Zhao et al. and Liu et al. [8,9] reported that a significant amount of P could be released from PR powder through microcrystallization treatment. The microcrystallization technology refers to the deep grinding of phosphate to a micron-sized level, decreasing the energy consumption [10]. Some activators have been used to accelerate and strengthen the transformation of P to bioavailable forms via chemical reactions and biological interactions [11].

Lignite is a typical activator that can decrease the angularity of PR powder particles and increase the proportion of middle-sized particles along with the reduction of dispersion [8,9]. The fineness of PR powder affects the effectiveness of P. Surface area and viscosity of humic acid in lignite are high, and the adsorption force is strong [12]. In the ultrafine pulverization of phosphate minerals, the addition of a high surface-reactive P activator such as lignite plays an important role in improving the product performance [13]. The positive effect of humic acid by lignite addition was confirmed by the generation of effective P applied to the soil [14]. Lignite humic acid was used to modify PR powder to prepare humic acid-activated phosphate fertilizer.

The effect of microcrystallization on the performance of PR has been evaluated by previous studies [15,16]. However, few correlation analyses of the properties of PR powder after microcrystallization have been reported, especially after adding lignite [17]. In this study, humic acid-activated phosphate fertilizer was prepared by microcrystallization to use the PR powder as a raw material and lignite as an activator. The relationship between the mineral characteristics of PR and P availability from plant cultivation was assessed. The particle size, specific surface area, and granule morphology of PR were analyzed. The effects of microcrystallinity on PR powder and lignite humic acid during the preparation of humic acid-activated phosphate fertilizer were evaluated. After activation, the surfaces of PR particles are covered with organic molecules. This significantly increases the surface exposure to the soil matrix and enhances the physical, chemical, and biological reactions on PR surfaces, thus ensuring a continuous release of P and a subsequent increase in the utilization efficiency [18]. Compared with traditional P fertilizer production using acids, the activation method used in this study has several benefits, such as minimal waste generation from production processes, beneficial use of medium-low-grade PR resources, low cost, and environmental friendliness [19].

2. Experimental Section

2.1. Raw Materials

In this study, raw materials containing Yunnan rock powder (PR, collophanite) were collected from Qingda Powder Material Engineering Co., Ltd., Zibo, Shandong, China. The main chemical composition of the phosphate sample is as follows: P₂O₅ 22.40%, CaO 32.69%, MgO 0.498%, SiO₂ 33.30%, Fe₂O₃ 1.98%, Al₂O₃ 5.02%, K₂O 0.899%, Na₂O 0.2%, F 1.21%, SO₃ 0.278%, MnO 0.862%, TiO₂ 0.198%, Na₂O 0.172%, NiO 0.130%, Cl 0.09%, SrO 0.0756%, ZnO 0.0472%, Cr₂O₃ 0.0301%, BaO 0.0640%, Y₂O₃ 0.0136%, PbO 0.0131%, V₂O₅ 0.0115%, ZrO₂ 0.0095%, and HgO 0.0068%, belonging to medium-low-grade phosphate mineral. In this study, 100-mesh with a jaw crusher and a normal grinder were separately used for pretreatment of PR. Lignite was obtained from White Lawn village, Ningwu county, Xinzhou city, Shanxi province, China. PR and lignite were also microcrystallized. The performance of prepared samples was characterized and analyzed for dry matter and available P by potted experiments.

2.2. Sample Preparation

The PR powder samples with different dosages (1%, 2%, 3%, and 5%) of lignite were treated using microcrystalline equipment (WJH-02), custom-built by Tsinghua University. The tank volume of milling equipment was 2 L, and the medium contained steel balls. The mass fractions of slurry concentration with different dosages of lignite were 47.5%, 50.0%, 52.2%, and 56.0%. Grinding time was set at 5, 10, 15, 20, 25, 30, 45, 60, 75, 90, 105, 120, 135, and 150 min. Samples were dried at 105 °C for characterization and chemical analysis. And samples for XRD testing were sieved with a sieve of 200-mesh to remove big particles.

Pot cultivation tests for plant growth were conducted at a glasshouse in Tsinghua University Organic Fertilizer Base in Beijing. A soil (aqui-cinnamon soil) with pH 8.2, and organic matter 11.7 g/kg was used for pot cultivation. The available phosphorous, potash, and nitrogen contents were 18.2, 205.2, and 67.0 mg/kg, respectively. Three treatments, control (No P), raw PR powder (PR1) 16 g/pot, and microcrystallized PR powder with lignite (PR2) 16.0 g/pot, were compared. Each treatment was repeated three times and randomly arranged. Rapeseed seeds were treated with hot water for 15 min and germinated at 25 °C for 3 days. The growth time was 57 days, and three strains were used as samples after harvest. All the standard cultivation practices were followed. The weights of biomass after harvest were noted, and post-harvest soil samples were analyzed to determine the available P content.

2.3. Characterization

XRF (X Ray Fluorescence, PFX-235 Rh 60kV LiF200 LiF220 Ge111 AX03) was used to characterize the elemental composition of the sample. Particle-size distribution was measured using a JL-6000 laser particle-size analyzer (range of measurement: 0.02–2000 μm, repeatability of $D_{50} \leq \pm 3\%$ standard powder). Specific surface area was measured using a JB-5-type surface area analyzer (according BET equation, the specific surface area of sample can be calculated by its absorbed single layer N_2) method, 0.0005 m²/g to no upper limit, repeatability of specific surface area $\leq \pm 3\%$ standard powder). The BET specific surface area measurement [20] was carried out as follows: The adsorbent was adsorbed on a solid surface at liquid nitrogen temperature (−195.8 °C). When the nitrogen molecules were in contact with the solid surface (m²/g, cm²/g) [21], the specific surface area was obtained by calculating the total surface area of 1 g of material from the cross-sectional area of nitrogen molecules. Scanning electron microscopy (SEM) was conducted using a KYKYSEM6200 microscope (SE Detector: 4.5 nm@30 kV, negative amplification: 15–250,000×). The citric acid-soluble P was assessed from the soluble P₂O₅ content in 2% citric acid solution using the Bulgarian State Standard 13418-80 [22]. The soil-available P in different treatments was measured using a 722S spectrophotometer (wavelength range 340–1000 nm). The data were analyzed using statistical software (SPSS software, 17.0, SPSS Institute Inc., USA) [23]. All treatment effects were determined using Duncan's multiple-range test. Significant treatment effects are presented at $P \leq 0.05$.

3. Results and Discussion

3.1. Effects of Microcrystallinity on the Particle Characteristics of PR Powder

3.1.1. Particle Size of PR Powder

Particle size refers to the dimension of length, and D_{50} and D_{97} represent the two characteristic particle sizes of the powder, as a distribution of 50% and 97%. D_{50} is often used to represent the average particle size of a powder sample; D_{97} is commonly used to represent the particle size of a coarse sample [24].

Because of the high grinding efficiency of the microcrystallization equipment, the particle sizes D_{50} and D_{97} of the PR powder sample first rapidly decreased during 25 min and then slowly decreased with the increase in grinding time as shown in Figure 1, much similar to another study [25]. Compared with

the raw PR powder, the D_{50} and D_{97} of 25 min PR powder decreased by 94.2% and 81.8%, respectively. Thus, the body strength increased [26]. The higher the surface energy, the higher the accumulation between particles, and the larger the particle size. When the two effects [27,28] were combined at a certain time, microcrystallinity and particle accumulation reached a dynamic equilibrium, and the particle size became stable. After 60 min of grinding, the particle size D_{50} slowly decreased, whereas the particle size D_{97} sharply increased up to 120 min, reaching a particle size of up to 34.3 μm . When the PR powder was ground for 30 min, the particle sizes D_{50} and D_{97} were 1.9 μm and 18.0 μm , respectively. The equipment processing efficiency was very low from 30 min to 60 min; the particle sizes D_{50} and D_{97} were 1.5 μm and 13.8 μm at 60 min, respectively.

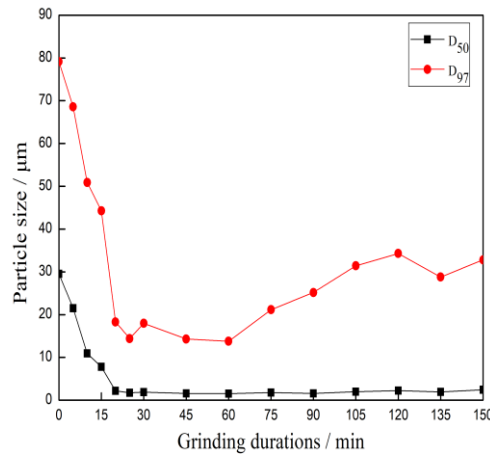


Figure 1. Particle size of phosphate rock (PR) powder at different grinding durations.

3.1.2. Particle Size Uniformity of PR Powder

The uniformity coefficient (fractal dimension) is an indicator of the particle-size distribution of a powder sample, and it is also one of the important parameters to evaluate the quality and use of mineral powder products. Fractal dimension and particle-size distribution are positively correlated. The larger the fractal dimension, the wider the particle-size distribution, and the narrower the distribution width. According to fractal theory, the fractal dimension of particle-size distribution can be expressed as follows [29]:

$$\ln S(D) = \ln K + (3 - F) \cdot (\ln D - \ln D_{max}) \quad (1)$$

where $S(D)$ is the particle-size cumulative distribution function, unit %; K is a constant; F is the fractal dimension of particle-size distribution, a dimensionless constant; D is the particle size, unit μm ; D_{max} is the maximum particle size, unit μm .

Using $\ln S(D)$ for the y -axis and $(\ln D - \ln D_{max})$ for the x -axis, 11 characteristic particle sizes D_{03} , D_{06} , D_{10} , D_{16} , D_{25} , D_{50} , D_{75} , D_{84} , D_{90} , D_{97} , and D_{98} of PR powder and different traits (F) were calculated using Equation (1). The results are shown in Figure 2.

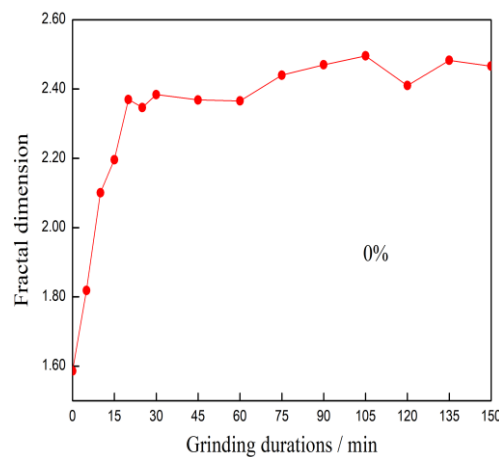


Figure 2. Fractal dimension of PR powder at different grinding durations.

With the increase in grinding duration, the fractal dimension of PR powder particle size gradually increased. Because the PR powder could be easily pulverized, the particle size of PR powder particles rapidly decreased at the beginning of grinding, whereas the large particles did not completely disappear, still accounting for a considerable proportion. The width of particle-size distribution gradually widened and can be expressed as an increase in fractal dimension. As the grinding continued, the proportion of larger particles gradually decreased, and the proportion of particles ($d \leq 1.0 \mu\text{m}$ and $d \leq 10 \mu\text{m}$) gradually increased. Because of the accumulation of particles and cladding effects of lignite on PR powder, the particle-size distribution became stable after 45 min.

In general, for particles with fractal boundaries (whose local and overall morphology are similar and don't vary with magnification), the fractal dimension can be used to describe their shape. The larger the fractal dimension, the rougher the grain contour [30]. The fractal dimension of PR powder and the roughness of particles increased with the increase in grinding duration, and the variation in roughness after 45 min of grinding was smaller than that in the beginning of grinding. The sedimentary phosphate rock has a fractal structure, and the surface has uneven areas. The relatively small concave area reflects the active point on the surface of the phosphate rock. During the beginning 30 min of the crushing process, the main change was that the large particles became small particles. Big particles were mainly broken along fractal structure and the fracture surface of the particles was uneven, and the fractal dimension gradually increased. After 30 min, particles broke slowly, and their shape change was the main change. The shape corners of the particles were removed by friction and fine particles adhered to the surface of the big particle curves. The fractal dimension showed a downward trend [31].

3.1.3. Homogeneous Degree of PR Powder

Uniformity represents the degree of particle size: the closer to 1, the better [32]. The results of $(D_{90}-D_{10})/D_{50}$ are shown in Figure 3. With the increase in grinding duration, the particle size of PR powder as a whole rapidly decreased, followed by a slow decrease and slight increase in the end. The particle size slowly decreased continuously from 30 min to 60 min. The finer the particles, the higher the surface energy, and the greater the tendency of accumulation between particles. The change in particle size depends on the combined effect of these two effects [33]. With the increase in grinding duration, the homogeneity of PR powder gradually increased in the first 30 min and then slightly decreased until 60 min. Gai [34] reported that the initial particle size was large, and the interaction between particles was small. With the increase in grinding duration, the particle size became smaller, and the interaction between particles increased. Thus, the combined phenomenon was observed. When the crushing time was short, many coarse large particles were present; only a small part of the very fine particles was present. With the increase in grinding duration, more and more

small particles were produced. The particle size became smaller and smaller, and the uniformity also decreased. The distribution of particles was more and more narrow.

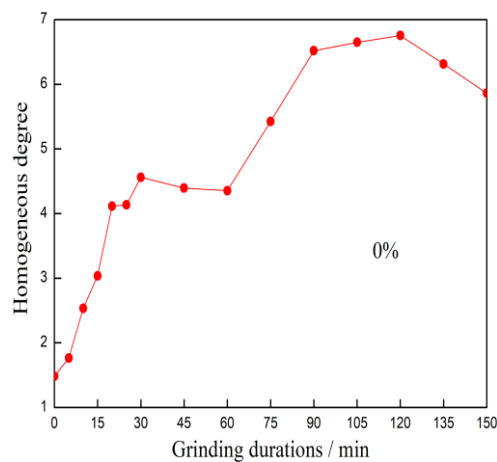


Figure 3. Homogeneous degree of PR powder at different grinding durations.

3.1.4. Correlation between Specific Surface Area and Characteristic Particle Size of PR Powder

The specific surface area and characteristic particle size (such as D_{10} , D_{50} , D_{90} , and D_{97}) of a powder are often used as characteristic indexes to characterize the thickness of powder. The specific surface area of PR powder was the surface area of unit powder, completely reflecting the thickness of PR powder.

The median diameter D_{50} was selected as the characteristic particle size of PR powder to study the correlation between specific surface area and characteristic particle size of PR powder, as shown in Figure 4. The specific surface area of PR powder was negatively correlated with particle size, following the logistic equation.

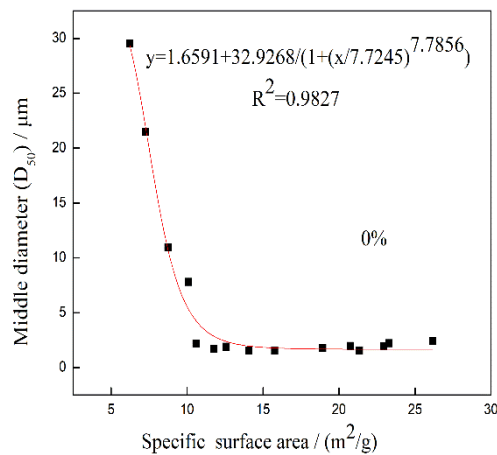


Figure 4. Correlation between specific surface area and middle diameter of PR powder.

3.1.5. Roughness and Specific Surface Area of PR Powder

The specific surface area of PR powder was measured using the BET method, and the specific surface area calculated from the particle size was compared. Figure 5 shows that with the increase in grinding duration, the difference in PR powder specific surface area shows an increasing trend, and the surface roughness increases. This is because in most cases, the powder particles were not smooth isometric particles. They were composed of particles of different particle sizes, and the surface state of these particles was not the same. They developed inner and outer surfaces, including the surface of particles raised, concave parts, fissures, microslits, and walls of pores and cavities, that are

in contact with the surface of particles. These surface areas add up to several times or several orders of magnitude larger than the surface area of an equal-diameter smooth sphere. Therefore, by comparing the difference between the specific surface area calculated using the BET method and that calculated from the particle size, the roughness of particle surface can be generally reflected [35].

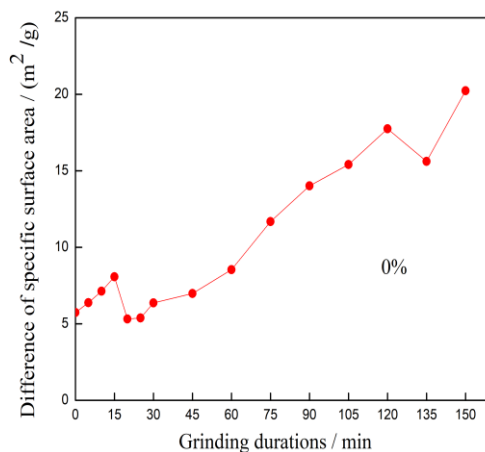


Figure 5. Difference in specific surface area of PR powder at different grinding durations.

Figure 6 shows the correlation between specific surface area and roughness of PR powder. The greater the specific surface area, the greater the roughness of PR powder.

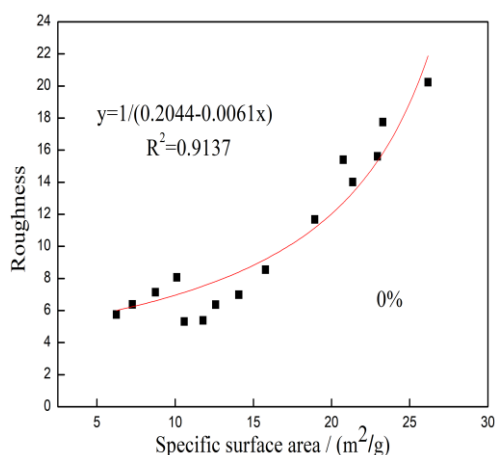


Figure 6. Correlation between specific surface area and roughness of PR powder.

3.1.6. XRD Patterns of PR at Different Milling Times

Figure 7 shows the mineral phases present in the sample are fluorapatite [$\text{Ca}_5(\text{PO}_4)_3(\text{F},\text{OH})$] and quartz (SiO_2), as confirmed by XRD analysis. The diffraction peaks from both phases in the PR sample changed clearly. Although the PR sample came from weathered PR, which had bad crystal and low diffraction peaks of [$\text{Ca}_5(\text{PO}_4)_3(\text{F},\text{OH})$], compared to the raw materials, the (002), (211), and (300) crystal face diffraction peaks of [$\text{Ca}_5(\text{PO}_4)_3(\text{F},\text{OH})$] clearly decreased. Whereas the diffraction peaks of the quartz, the (011) crystal faces, decreased significantly during milling time.

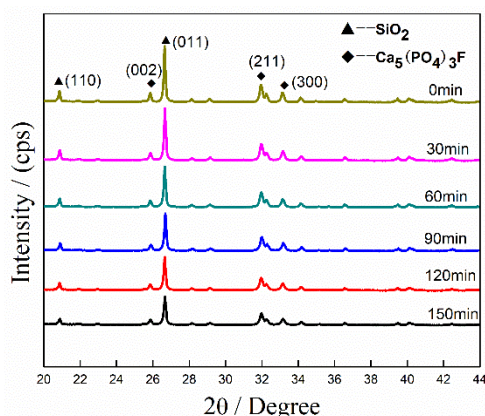


Figure 7. XRD patterns of PR at different milling times.

3.2. Effects of Adding Lignite on Particle Characteristics of PR Powder

3.2.1. Size Distribution of PR Powder with Lignite Addition

A pile of dispersed powders consisting of many particles of different sizes was not quantified through individual particles but the particle-size distributions. Figure 8 shows typical particle-size distributions obtained using a laser particle size analyzer for different grinding durations of PR powder: 0.0, 0.1, 0.2, 0.5, 1.0, 2.0, 5.0, 7.3, 10.0, 10.9, 16.3, 18.7, 20.0, 24.4, 27.8, 47.5, 50.0, 70.9, and 100.0 μm . Grinding changed the particle-size distribution of PR powder without lignite significantly in a large region. The composition ratio of particles ($d \leq 1.0 \mu\text{m}$ and $d \leq 10 \mu\text{m}$) first rapidly increased and then gradually decreased because big particles were broken, and the small ones adhered to the big ones. The values were 30.3% and 91.5% at 30 min, respectively. At 30 min, the change in particle size was small, and these values were 36.1% and 94.4% more than those of the raw PR powder, respectively; and the values increased by 36.1% and 92.2% at the maximum duration of 60 min, respectively.

However, compared with the raw PR powder and lignite, the composition ratio of particles ($d \leq 1.0 \mu\text{m}$ and $d \leq 10 \mu\text{m}$) of the PR powder added with 1%, 2%, 3%, and 5% lignite changed significantly, first increasing and then gradually decreasing. With the increasing amount of added lignite, the grinding duration of PR powder particles ($d \leq 1.0 \mu\text{m}$ and $d \leq 10 \mu\text{m}$) reaching the maximum was different. With the addition of 1%, 2%, and 3% lignite, the grinding duration decreased to 25 min, 15 min, and 20 min, respectively, accounting for 30.3%, 9.8%, and 20.6% of particles ($d \leq 10 \mu\text{m}$), respectively, and 90.2%, 77.5%, and 87.7% of particles ($d \leq 1.0 \mu\text{m}$), respectively. However, with the addition of 5% lignite, the grinding duration was 60 min, accounting for 41.9% of particles ($d \leq 1.0 \mu\text{m}$) and 85.4% of particles ($d \leq 10 \mu\text{m}$). This was the optimal activation effect on the particles obtained by adding 3% lignite to PR powder in an appropriate grinding duration (20 min).

Grinding altered the distributions of the mixture (PR and lignite) by decreasing particle sizes. For every treatment, the mixture with 5% and 3% lignite contained the higher ratio of particles whereas the mixture with 2% and 1% lignite contained the lower ratio due to the release of citric acid-available P in higher quantity, meaning that the mixture with 5% and 3% lignite released more citric acid-available P than the mixture with 2% and 1% lignite. The mechanism is perhaps that lignite prevented small particles adhering to the big ones.

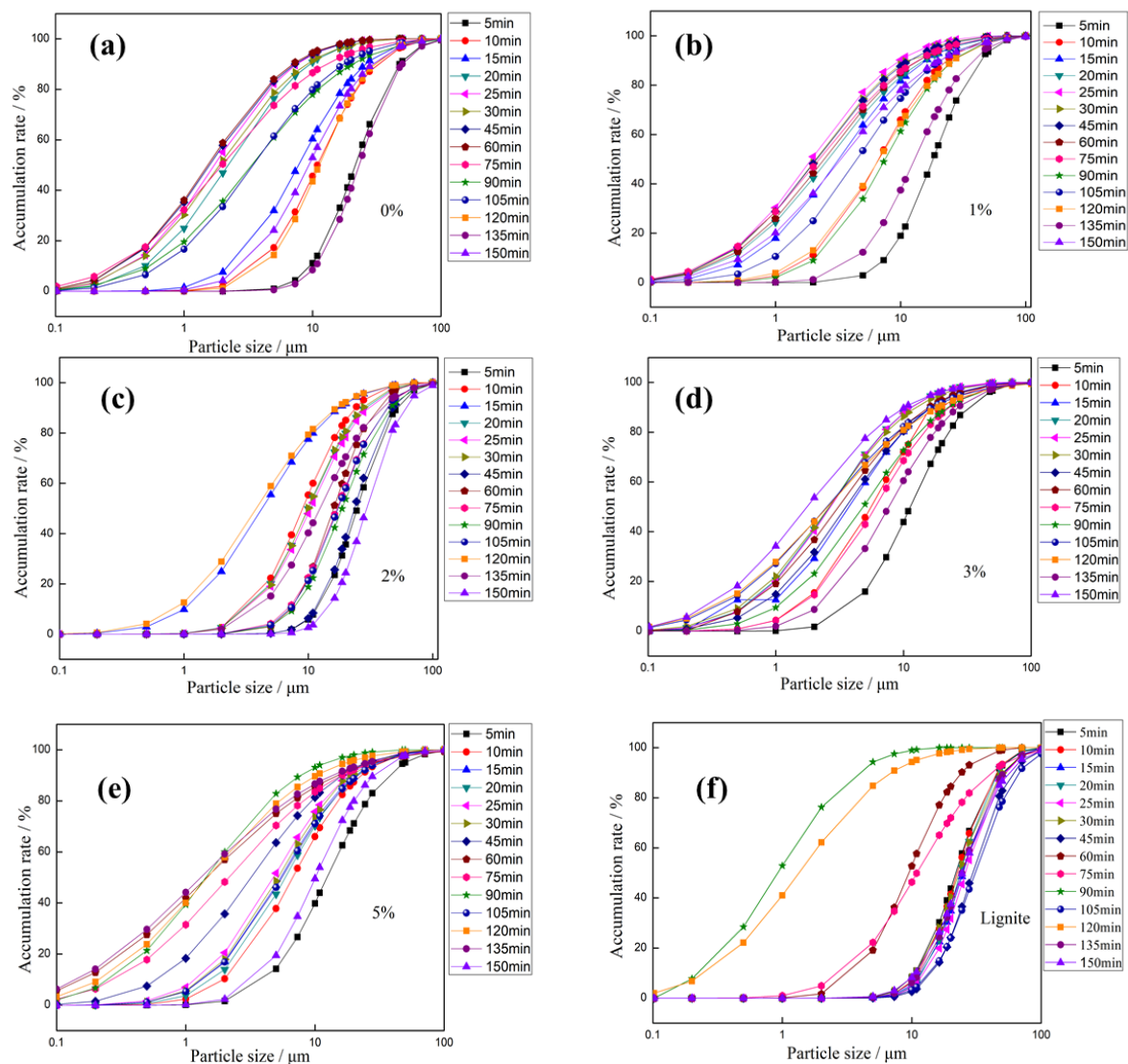


Figure 8. Size distribution of PR powder at different grinding durations.

3.2.2. Effect of Lignite Addition on Particle Size (D_{50} , D_{97})

Figure 9 shows that the characteristic particle size (D_{50} , D_{97}) of PR powder added with 1%, 2%, and 3% lignite first rapidly decreased during 20 min and then slowly decreased until 105 min, and a peak appeared at 135 min, followed by a sharp drop to 150 min. Compared with other treatments, the D_{50} and D_{97} of treatments with the addition of 5% lignite was significantly different, which first decreased exponentially during 30 min and then slightly decreased until 90 min. A sharp rise was observed until 150 min. Addition of 5% lignite had an inhibition effect on the decreasing (D_{50} , D_{97}) of PR powder. The microcrystallization process not only decreases the particle size of lignite, but also activates the lignite. According to 21 lignite statistics, the total humic acid in the free humic acid-based sample accounts for about 80–99% [36]. Because of the presence of free humic acid molecules containing many carbonyl, phenolic hydroxyl, quinone, and other functional groups as well as metal ions, oxides, minerals, and organic substances including toxic and harmful substances, the environmental chemical behavior of these substances can be affected [37]. These behaviors mainly include the following: (1) Adsorption: Lignite contains humic acid in the porous sponge-like structure, and the molecular structure contains many active groups, providing a large surface area, high viscosity, and good adsorption properties [38]. P powder coating and other complex factors such as pellet agglomeration, grain refinement, and particle agglomeration are used to achieve a dynamic balance, so that the

difficulty of smashing increases. (2) Decomposition: Humic acid promotes the decomposition of PR powder, so that water-insoluble P is converted into water-soluble P, benefiting crop absorption. (3) Complexation: An increase in the solubility of apatite in the presence of humic acid can be attributed to the formation of P-HA (humic acid) complex. IR (infrared) and PNMR (proton nuclear magnetic resonance) analyses confirm the presence of such complexes that immobilize and activate the nutrients in soil and fertilizer under suitable pH conditions [39].

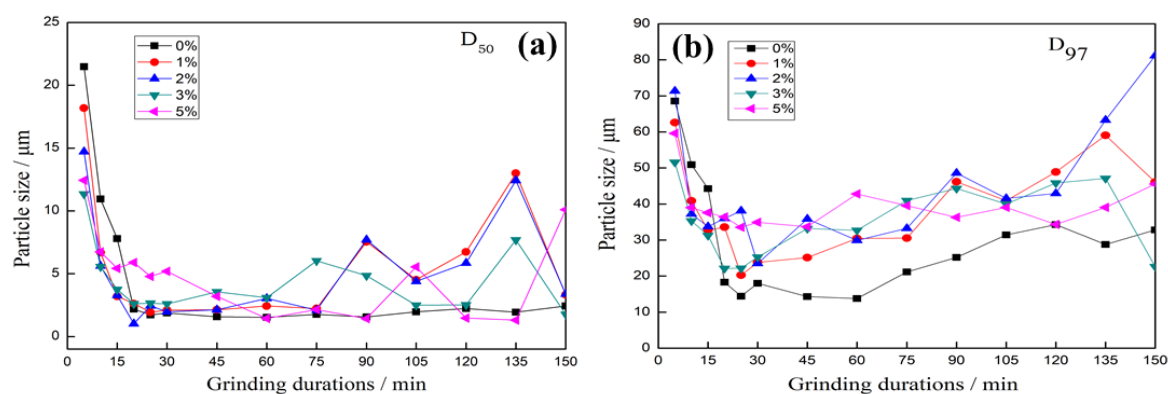


Figure 9. Particle size of PR powder after adding different amounts of lignite at different grinding durations.

3.2.3. Effect of Lignite Addition on Specific Surface Area of PR Powder

Specific surface area is an indicator of the macroscopic fineness of a powder [24]. After adding 1%, 2%, 3%, and 5% lignite, the specific surface area of the sample was measured, and the results are shown in Figure 10. A positive correlation was observed between the specific surface area of samples after different treatments and grinding duration, which follows the langmuirEXT1 equation (0%, 5%) and allometric1 equation (1%, 2%, 3%), as shown in Table 1. According to the correlation equation, the specific surface area of all samples goes up until even. In the order of 0%, 1%, 2%, 3%, and 5% lignite to PR powder during 30 min, $5\% (15.0 \text{ m}^2 \cdot \text{g}^{-1}) > 2\% (14.2 \text{ m}^2 \cdot \text{g}^{-1}) > 1\% (13.2 \text{ m}^2 \cdot \text{g}^{-1}) > 3\% (13.1 \text{ m}^2 \cdot \text{g}^{-1}) > 0\% (12.6 \text{ m}^2 \cdot \text{g}^{-1})$. The addition of 5% lignite had the maximum effect on the specific surface area of PR powder during 30 min.

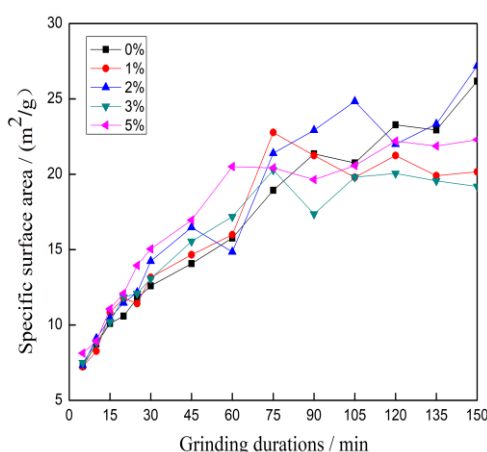


Figure 10. Specific surface area of PR powder after adding different amounts of lignite at different grinding durations.

Table 1. Correlation of specific surface area and grinding durations.

Amount of Lignite Addition	Correlational Equation	R ²
0%	$y = (3584.7444 * 8.8051x^{0.4138}) / (1 + 8.8051x^{0.4138})$	0.9768
1%	$y = 4.4540 * x^{0.3224}$	0.8780
2%	$y = 3.5655 * x^{0.3974}$	0.9419
3%	$y = 4.9526 * x^{0.2892}$	0.9271
5%	$y = (30.3630 * 0.0975x^{0.6786}) / (1 + 0.0975x^{0.6786})$	0.9682

After grinding for 30 min, without lignite, the specific surface area of PR powder rapidly increased until 90 min; after this fluctuation, it increased up to $26.2 \text{ m}^2 \cdot \text{g}^{-1}$ until 150 min. However, the addition of lignite decreased the efficiency of grinding, and the specific surface area of PR powder became smaller because of the agglomeration of granules and cladding effect of lignite on PR powder. Solid action through mechanical forces is often a combination of multiple phenomena and can be divided into two stages: (1) The particles hit themselves and rupture and become refined. The material surface area increases the crystallinity, lattice defects, and lattice displacement. Thus, the system temperature increases, and thus the free energy also increases. (2) The free energy decreases; therefore, the chemical potential energy of the system also decreases. The powder is agglomerated, and the specific surface area decreases. The material can be recrystallized, resulting in mechanical chemical effects [40].

3.2.4. Effect of Lignite Addition on Granule Morphology of PR Powder

PR powder has obvious fractures: the particles are plate-shaped with a smooth surface and dense structure. Figure 11 shows the SEM images of PR powder and lignite grinded for different times.

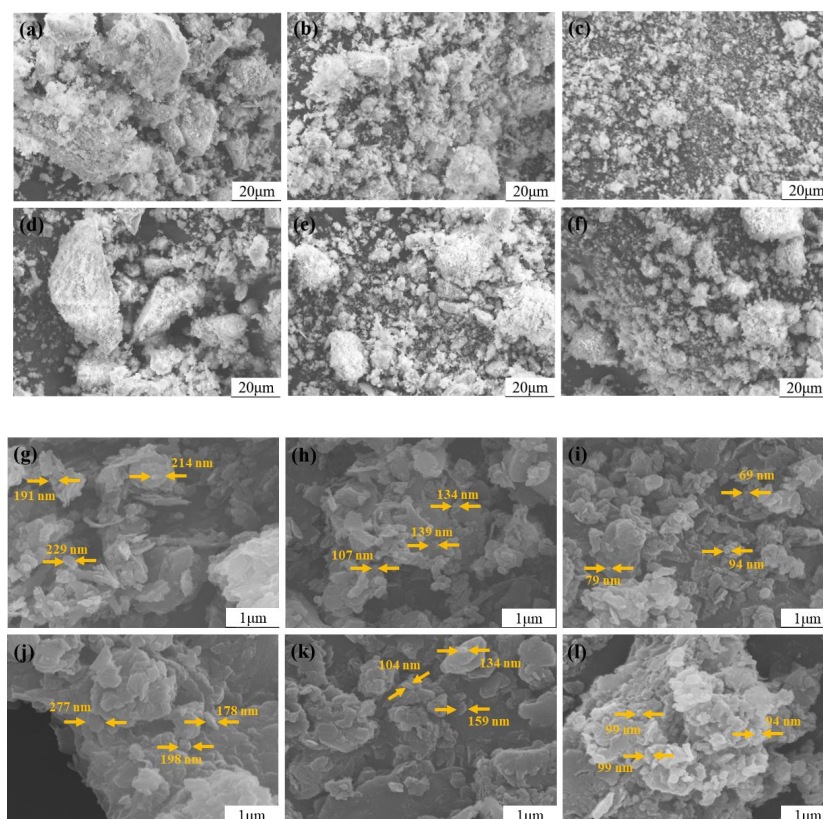


Figure 11. SEM images of PR powder and lignite at different grinding durations: PR powder raw material (a and g), microcrystalline PR powder 30 min (b and h) and 150 min (c and i). Lignite raw material (d and j), microcrystalline 3% lignite and PR powder 30 min (e and k) and 150 min (f and l).

The SEM images show that the particle sizes of PR powders are significantly different, as shown in Figure 11. After grinding for 150 min, the particle-size distribution is uneven with a relatively high dispersion. The large particles are predominant with less intermediate size particles, and the small particles have obvious agglomeration. This is closely related to the way in which the grinding medium acts on the material to generate forced vibration during the microcrystallization process. However, by extending the grinding duration, the particles rub against the grinding medium or against each other, and the angular edges of flaky particles are ground to form spherical or spheroidal particles. The particle-size distribution tends to be uniform, and the degree of amorphization increases.

With the addition of 3% lignite, the surface structural characteristics of PR powder are more distinct with the increase in grinding duration. The lignite raw material has many layers of particles, a large viscosity, different particle sizes, and a rough surface. There are a large number of primary cell pores, interchain pores, cracks, and pores in the particles. The pore-size distribution is wide, and the particle surfaces are rich in oxygen-containing functional groups. These pore structures and oxygen-containing functional groups make it easier for lignite to adsorb on the surface of PR powder particles during the grinding.

3.2.5. Effect of Lignite Addition on the Citric Acid-soluble P of PR Powder

The PR powder was added with 1%, 2%, 3%, and 5% lignite to make it microcrystalline, and the released amount of citric acid-soluble P in different treated PR powders was measured as shown in Figure 12. Compared with no addition of lignite, in the addition of lignite 1% and 2%, the release of citric acid-soluble P from PR powder was very low, whereas the addition of lignite 3% and 5% increased the citric acid-soluble P. The citric acid-soluble P of PR powder (+3% lignite) and PR powder (+0% lignite) was 6.7% and 3.0%, respectively, in 30 min grinding; PR powder (+3% lignite) increased the release of citric acid-soluble P by 125.3% at a grinding time of 30 min. This is the optimal proportion. It was observed that the activation is very weak with 1% and 2% lignite addition due to a slow decrease in particle size; however, the activation effect is stronger with the addition of 3% and 5% lignite in PR powder. In an acidic environment, the dissolution process is: $\text{Ca}_{10}(\text{PO}_4)_6\text{F}_2 + 12\text{H}^+ \rightarrow 10\text{Ca}^{2+} + 6\text{H}_2\text{PO}_4^- + 2\text{F}^-$; $\text{Ca}_{10}(\text{PO}_4)_3(\text{CO}_3(\text{OH}))_3\text{FOH} + 6\text{H}^+ \rightarrow 10\text{Ca}^{2+} + 3\text{H}_2\text{PO}_4^- + 3\text{CO}_3^{2-} + \text{F}^- + \text{OH}^-$. Hydrogen ions produced by humic acid in lignite can react with microcrystallization PR to promote the continuous release of phosphate ion [39]. Compared with water-soluble chemical phosphate fertilizer, phosphorus is not completely released at one time. The release of phosphorus from mineral phosphate fertilizer is slow, and the local concentration of phosphate ion can be avoided, resulting in the reduction of the effectiveness of trace elements such as zinc and iron affecting plant growth.

The correlations were observed between citric acid-soluble P of different treatments and grinding duration, which respectively followed the Linear equation (+0% lignite), Allometric equation (+1% lignite), Allometric equation (+2% lignite), Belehraddek equation (+3% lignite), Belehraddek equation (+5% lignite), as shown in Table 2 in the beginning 30 min. However, only the correlations of the samples (+0% lignite, +3% lignite, +5% lignite) were positive. The citric acid-soluble P of samples (+3% lignite, +5% lignite) increased significantly during the beginning 30 min. There are two causes of citric acid-soluble P increasing. First, the interaction of the surface phosphate with citric acid was easy since the particles of samples decreased, and specific surfaces increased during grinding. Second, lignite released H^+ , which activated PR. This function was rapid. However, lignite could adsorb phosphate ions through metal ions (Ca^{2+}) and thus decrease the P content dissolved in citric acid solution. The sites of lignite that combined with phosphate ions through metal increased during grinding and thus it made the decreasing trend of citric acid-soluble P. However, the phosphate combined with lignite is available to plants and it is not easy to be fixed to soil colloid [41].

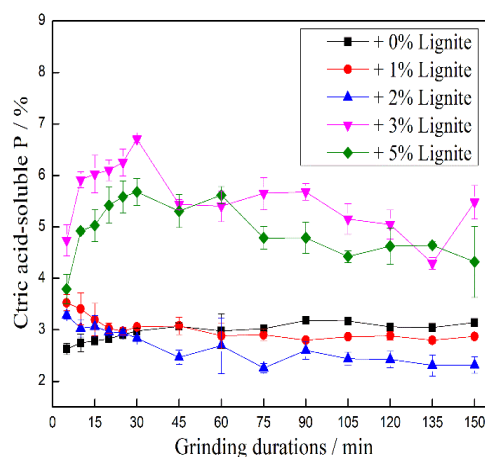


Figure 12. Changes in the citric acid-soluble P content of PR powder by adding different amounts of lignite at different grinding durations.

Table 2. Correlation of citric acid-soluble P and grinding durations.

Amount of Lignite Addition	Correlational Equation	R ²
0%	$y = 2.5850 + 0.0129x$	0.9671
1%	$y = 4.1666x^{-0.0985}$	0.8835
2%	$y = 3.6621x^{-0.0716}$	0.8851
3%	$y = 5.1623(x - 4.7002)^{*0.0704}$	0.9169
5%	$y = 4.0521(x - 4.4667)^{*0.1040}$	0.9790

3.2.6. Dry Matter from Rapeseed Growth, Available P inside Soil, and the N, P, K Uptake Content

P fertilizer effectiveness was determined in a pot cultivation test with the amounts of rapeseed biomass including both the aboveground plant part and the underground root. P application promoted the accumulation of dry matter in rapeseed, and with different treatments of rapeseed, the difference in dry matter was significant, as shown in Figure 13a. Compared with the control treatment, the dry matter of aboveground and underground parts of the PR1 treatment increased by 35.4% and 28.6%, respectively; with the PR2 treatment, an increase of 56.6% and 54.0% against the control, and an increase of 15.7% and 19.8% against PR1, respectively.

Regarding the total amount of rapeseed dry matter, significant differences were observed for different treatments. The maximum was obtained with the PR2 treatment: an increase of 56.1% compared with the control treatment. This indicates that the application of PR powder promotes the growth and development of aboveground and underground plants of rapeseed. The effect of microcrystalline-activated PR powder is stronger than that of ordinary PR powder. The data clearly indicate that microcrystalline grinding improves the effectiveness of PR powder, as shown in Figure 12. This is beneficial to the photosynthesis of rapeseed and promotes the accumulation of dry matter of rapeseed, as shown in Figure 13a.

The results show fertilizing microcrystallization PR increased the nutrient uptake of rape, as shown in Figure 13c. The content of available P in the treated soil considerably increased with microcrystallization processing; PR2 was higher than PR1 by 28.3%, whereas for PR2 and PR1 against the control, it significantly increased by 89.6% and 69.8%, respectively, as shown in Figure 13b. The application of PR powder has a significant effect on soil-available P in rapeseed. All differences reached a significant level. The treatments fertilizing PR increased the soil-available P level compared to the control, so that the rapeseed absorbed phosphorus easily, prompting other nutrients (N and K) to be absorbed. Since microcrystallization adding lignite made PR releasing phosphorus more easily, the rapeseed of treatment PR2 absorbed more P than other treatments. Proper application of PR powder could promote the growth and development of plants and could have a certain positive effect on alleviating the shortage of PR.

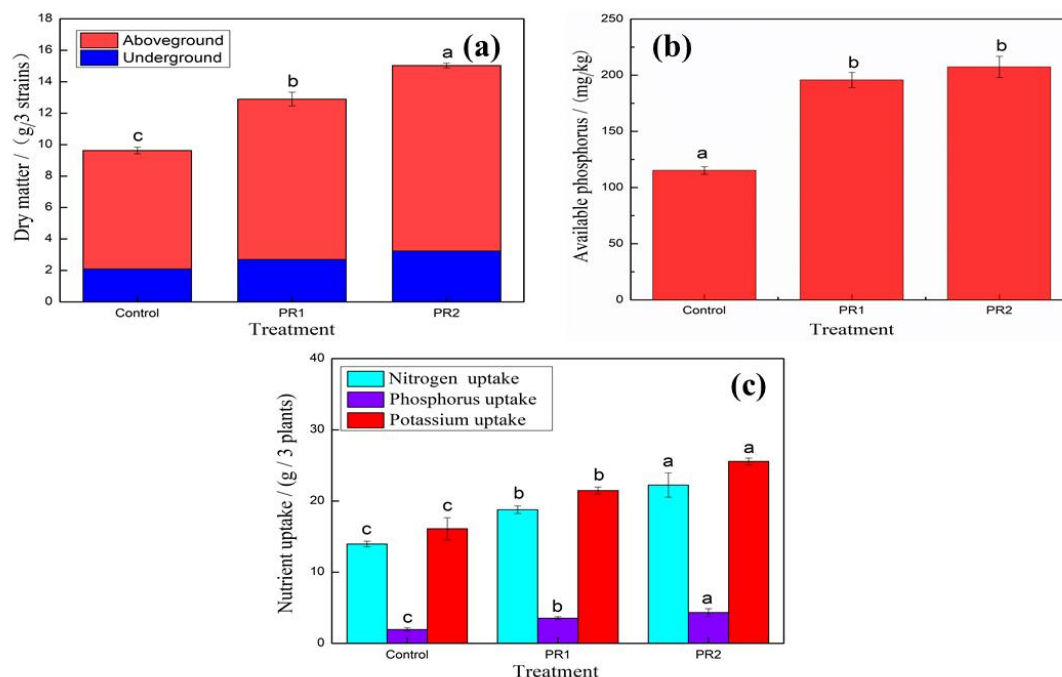


Figure 13. Dry matter (a), available P (b), and the N, P, K uptake content (c) of samples in different treatments (the different letters within a column showed statistically significant ($p < 0.05$)).

4. Conclusions

The microcrystallization operation significantly affected the particles, specific surface area, granule morphology, and the release of citric acid-soluble P of PR powder.

The microcrystallization decreased the (002), (211), and (300) crystal face diffraction peaks of $[\text{Ca}_5(\text{PO}_4)_3(\text{F},\text{OH})]$ and changed its crystal.

For PR powder, grinding primarily broke big particles along the fractal structure so that the PR fractal dimension was increased. Then the grinding cut the corners of particles and made fine particles adhered to big ones. PR powder D_{50} primarily decreased, and then went smoothly, whereas, its fractal dimension went up and then changed slowly. Correspondingly, the particle homogeneous degree nearly showed the same trend as the fractal dimension. In 150 min grinding time, the specific surface area went up all the time.

With the addition of lignite (1% and 2%), the particle-size distribution of PR powder became complicated, and produced less fine particle ratio (diameter $\leq 1 \mu\text{m}$) and released less citric acid-available P. PR powder with 3% and 5% added lignite prevented fine particles from adhering to big ones when grinding and so they produced a large amount of independent particles and released more citric acid-available P.

Fertilizing lignite-active PR powder improved soil-available phosphorus content and rape promptly absorbed phosphorus and N, P nutrient elements. Additionally, rape production was increased, too.

Author Contributions: X.-m.Z., Z.-q.H., Z.-h.H., Y.-f.Y., X.-Y.H., and X.-y.L. conceived and designed the experiments; X.-m.Z. performed the experiments; X.-m.Z., Y.L., C.H., and M.-x.W. analyzed the data; G.-s.G. contributed reagents/materials/analysis tools; X.-m.Z. wrote the paper. G.-s.G., Z.-h.H., X.-y.L., and X.-Y.H. provided project support.

Acknowledgments: This work was financially supported by the National Natural Science Fund Project (Grant No. 51374136), National Key R&D Program of China (Grant No. 2017YFB0310801), Fundamental Research Funds for the Central Universities for Financial Support (Grant No. 2652017362), National Natural Science Foundations of China (Grant No. 51472222), National Key Research and Development Project (Grant No. 2018YFC1901503), and High-Level Talents Cross-Training in Beijing Colleges and Universities "Practical Training Plan" Graduation Design (Entrepreneurial) Support Plan (2017).

Conflicts of Interest: The authors declare no conflict of interest.

References

1. Van Vuuren, D.P.; Bouwman, A.F.; Beusen, A.H.W. Phosphorus demand for the 1970–2100 period: A scenario analysis of resource depletion. *Global Environ. Change* **2010**, *20*, 428–439. [[CrossRef](#)]
2. Cordell, D.; Rosemarin, A.; Schroder, J.J.; Smit, A.L. Towards global phosphorus security: A systems framework for phosphorus recovery and reuse options. *Chemosphere* **2011**, *84*, 747–758. [[CrossRef](#)] [[PubMed](#)]
3. Schroder, J.J.; Smit, A.L.; Cordell, D.; Rosemarin, A. Improved phosphorus use efficiency in agriculture: A key requirement for its sustainable use. *Chemosphere* **2011**, *84*, 822–831. [[CrossRef](#)] [[PubMed](#)]
4. Tao, Y.H. Quantitative relation formula of main chemical components in Cambrian phosphoric ore. *Yunnan Geol.* **1997**, *16*, 59–67.
5. Abbasi, M.K.; Mansha, S.; Rahim, N.; Ali, A. Agronomic effectiveness and phosphorus utilization efficiency of rock phosphate applied to winter wheat. *Agron. J.* **2013**, *6*, 1606–1612. [[CrossRef](#)]
6. Cevik, U.; Baltas, H.; Tabak, A.; Damlad, N. Radiological and chemical assessment of phosphate rocks in some countries. *J. Hazard. Mater.* **2010**, *182*, 531–535. [[CrossRef](#)] [[PubMed](#)]
7. Sun, X.; Meng, L.; Shi, Y.L. Studies on effectiveness of mechanical activated phosphate rock powder. *J. Jilin Agri. Sci.* **2014**, *39*, 47–50.
8. Zhao, F.T.; Gai, G.S.; Jing, D.W.; Yang, Y.F.; Dong, Y.J.; Liu, C.S. Ultrafine grinding activations of phosphate rock and their dynamic phosphorus releases. *Plant Nutr. Fert. Sci.* **2009**, *15*, 474–477.
9. Liu, F.C.; Xu, Z.; Ma, Y.M.; Xing, S.J.; Du, Z.Y.; Ma, H.L.; Ma, B.Y. Effects of ultra-fine rock phosphate rock powder on the poplar growth and different forms of soil phosphorous content. *Chin. Agri. Sci. Bull.* **2014**, *30*, 59–63.
10. Minjigmaa, A.; Temuujin, J.; Khasbaatar, D.; Oyun-Erdene, G.; Amgalan, J.; MacKenzie, K.J.D. Influence of mechanical distortion on the solubility of fluorapatite. Influence of mechanical distortion on the solubility of fluorapatite. *Miner. Eng.* **2007**, *20*, 194–196. [[CrossRef](#)]
11. Zhu, J.; Li, M.; Whelan, M. Phosphorus activators contribute to legacy phosphorus availability in agricultural soils: A review. *Sci. Total Environ.* **2018**, *612*, 522–537. [[CrossRef](#)] [[PubMed](#)]
12. Li, W.; Zou, L.Z.; Zhu, S.Q.; Qian, F.F. The general statement on humic acid application in recent ten years. *Humic Acid.* **2015**, *3*, 3–8.
13. Cheng, L.; Zhang, B.; Hou, C.H.; Chen, K.K.; Wang, J.; Shi, Y.L. Preparation and characteriation of nanoscale humic acid under high shearing condition. *CIESC J.* **2012**, *63*, 2648–2654.
14. Beck, M.H.; Escosteguy, P.A.V.; Dick, D.P. Modifications of phosphorus in Latosol as a function of humic acids and acidity. *Rev. Bras. Eng. Agr. Amb.* **2018**, *22*, 488–492. [[CrossRef](#)]
15. Lv, L.F.; Li, X.Y.; Zhang, H.W.; Dou, X.X.; Gai, G.S. Mechano-chemical effects of phosphorite on superfine grinding in ball-stirring mill in wet. *Acta Mineral. Sin.* **2016**, *36*, 382–386.
16. He, Z.Q.; Liu, C.S.; Gai, G.S.; Yang, Y.F.; Dong, Y.J.; Zhao, F.T. Effect on phosphorus availability of rock PR powder by grinding it superfine. *J. Soil. Water Conserv.* **2009**, *23*, 210–212.
17. Xu, Z.; Sun, Y.T.; Jing, D.W.; Liu, F.C. Application research on different activator in the preparation of superfine phosphate rocks. *Biol. Disaster Sci.* **2015**, *38*, 166–169.
18. Huang, L.; Mao, X.Y.; Wang, J.; Huang, D.M.; Lin, J.H.; Liao, Z.W. Phosphorus availability and fertilizer efficiency of rock phosphate as affected by ultrafine activation. *Acta Pedo. Sin.* **2013**, *50*, 143–151.
19. Mao, X.; Lu, Q.; Mo, W.; Xin, X.; Chen, X.; He, Z. Phosphorus Availability and Release Pattern from Activated Dolomite phosphate rock in Central Florida. *J. Agric. Food Chem.* **2017**, *23*, 4589–4596. [[CrossRef](#)]
20. Langmuir, I. The adsorption of gases on plane surfaces of glass, mica and platinum. *J. Am. Chem. Soc.* **1918**, *40*, 1361–1403. [[CrossRef](#)]
21. Salvestrini, S. Analysis of the Langmuir rate equation in its differential and integrated form for adsorption processes and a comparison with the pseudo first and pseudo second order models. *Reac. Kinet. Mech. Cataly.* **2018**, *123*, 455–472. [[CrossRef](#)]
22. Petkova, V.; Pelovski, Y.; Dombalov, I.; Kostadinova, P. Influence of triboactivation conditions on the synthesis in natural phosphate-ammonium sulphate system. *J. Therm. Anal. Calorim.* **2005**, *80*, 709–714. [[CrossRef](#)]
23. Lu, W.D. *SPSS for Windows tongji fenxi*, 2nd ed.; Electronic Industry Press: Beijing, China, 2004; p. 50.
24. Lv, L.F. Effects of microcrystalline grinding on potassium release in silicate potassium rocks and its application. Ph.D. Thesis, Shandong Agricultural University, Taian, China, 2014.

25. Zhu, Z.S.; Luo, Z.F.; Yang, Y.F.; Gai, G.S.; Lv, L.F.; Yu, X.D.; Wang, K.; Zhao, J.B. Experimental research on microcrystallizing processing of potassic shale. *J. China Univ. Min. Techno.* **2012**, *41*, 293–298.
26. Li, Z.J.; Qiao, G.G.; Mi, X.Y.; Chen, G.; Wang, Y.L. Energy savings during magnetite ore preparation in eastern Hebei province. *J. China Univ. Min. Techno.* **2008**, *37*, 625–629.
27. Jian, M. Primary approach to the relationship between powdering time and particle size in the process of superfine powdering. *Min. Res. Dev.* **1999**, *19*, 44–45.
28. Zheng, S.L.; Du, G.X.; Li, Y.; Huang, Y.L. Study on preparation of superfine tourmaline powder and its properties of negative ion disengagement. *Ming. Metall.* **2004**, *13*, 50–53.
29. Zhu, Z.S.; Luo, Z.F.; Yang, Y.F.; Gai, G.S.; Wang, X.X.; Wang, D.; Zhao, F.T. Fractal representation of particle-size distribution in the grinding of potassium-containing shale. *Ind. Miner. Process.* **2011**, *40*, 8–11.
30. Liu, D.J.; Zhong, B.H.; Zhang, Y.X. Surface fractal of phosphate rock and their reactivity. *Chem. React. Eng. Tech.* **1999**, *15*, 97–103.
31. Zhang, X.N.; Sun, Y.Y. Fractal Dimension calculation for rock surface texture. *Comput. Eng.* **2010**, *36*, 277–279.
32. Du, Y.; Zhao, L.J.; Feng, Y.; Xu, D.S.; Li, X.H.; Wang, S.T. Characterization methods of flow ability of traditional Chinese medicine powders. *China J. Chin. Mater. Med.* **2012**, *37*, 589–593.
33. Yuan, W.J.; Zhou, Y.M. Reasons for aggregation of nanoparticles and solutions. *Mater. Rev.* **2008**, *22*, 59–61.
34. Gai, G.S. *Powder Technology*; Tsinghua University Press: Beijing, China, 2009; pp. 82–84.
35. Tan, L.X.; Cai, Y.X.; Ding, Y.; Liang, T.R. Preliminary study on relationship of size determination by powder sedimentation method and BET specific surface area. *Chin. Process Eng.* **2002**, *2*, 20–23.
36. Chen, C.J. Briquettes compressive and moisture re-adsorption feature of upgraded lignite. Master Thesis, China University of Mining and Technology, Xuzhou, China, 2014.
37. Zhang, Y.F.; Huang, L.P. Research progress of humic acids in the treatment of environmental pollutants. *Humic Acid* **2007**, 16–20.
38. Trubetskaya, O.; Trubetskoj, O.; Richard, C. Photodegrading properties of soil humic acids fractionated by SEC-PAGE set-up. Are they connected with absorbance? *J. Photochem. Photobiol. A* **2007**, *189*, 247–252. [[CrossRef](#)]
39. Dai, Q.J.; Zhang, B.L.; Cheng, L.; Zhu, F.T.; Dong, Q.Y.; Yuan, L. Efficacy and application of phosphate fertilizer containing humic acid. *Phosphate Compd. Fert.* **2012**, *27*, 5–7.
40. Yang, N.R. Influence of mechanical distortion on the solubility of fluorapatite. *Miner. Eng.* **2007**, *20*, 194–196.
41. Rao, W.; Wang, S.Y.; Liu, F.; Wang, D.Z. Characteristics of dissolution kinetics of phosphorus and calcium from phosphate rocks. *Chin. Agri. Sci. Bull.* **2007**, *23*, 224–227.



© 2019 by the authors. Licensee MDPI, Basel, Switzerland. This article is an open access article distributed under the terms and conditions of the Creative Commons Attribution (CC BY) license (<http://creativecommons.org/licenses/by/4.0/>).